

Upconversion Particle as a Local Luminescent Brownian Probe: A Photonic Force Microscopy Study

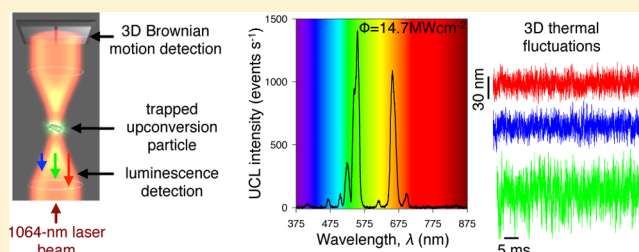
Flavio M. Mor,* Andrzej Sienkiewicz, László Forró, and Sylvia Jeney

Laboratory of Nanostructured and Complex Matter Physics (LPMC), Institute of Condensed Matter Physics (ICMP), Faculty of Basic Sciences (FSB), Ecole Polytechnique Fédérale de Lausanne (EPFL), CH-1015 Lausanne, Switzerland

Supporting Information

ABSTRACT: Near-infrared (NIR) light sensitive lanthanide-doped NaYF₄ upconversion particles (UCPs) are gaining increasing attention as local probes in biomedical applications. Here, we implemented a photonic force microscope (PFM) to manipulate and study the optical properties of trapped single UCPs, β -NaYF₄:Yb,Er. In particular, we focused on the mechanisms of the optical trapping of nonspherical UCPs of different sizes, in the range 0.5–2 μ m, as well as on their upconversion photoluminescence (UCL) properties under excitation with the strongly focused laser beam ($\lambda = 1064$ nm) of the PFM, operating at power densities up to 14.7 MW cm⁻². A careful analysis of UCL under such conditions points to three emission peaks at 469, 503.6, and 616.1 nm, which were enhanced by the high laser power density. The analysis of Brownian motion was used to quantify the thermal fluctuations of the particle inside the optical trap as well as the particle sizes and optical forces acting in the two dimensions perpendicular to the optical axis. A steep dependence of UCL as a function of the particle diameter was found for UCPs having sizes smaller than the focal spot (~ 900 nm) of the NIR laser.

KEYWORDS: β -NaYF₄:Yb,Er particle, optical trapping, optical tweezers, nonlinear optics, upconversion photoluminescence, Brownian motion



Life sciences have a constantly growing need for novel methodological approaches suitable to investigate the intracellular environment with increased time and spatial resolutions. Optical near-field probes, such as laser-illuminated metal tips, uncoated/metal-coated tapered optical fibers, and nanoemitters, such as single molecules or nanoparticles, have attracted increasing attention as key components of high-resolution microscopes.

In parallel, super-resolution fluorescence microscopy, operating in the far-field regime and overcoming the light diffraction limit, has markedly improved imaging resolution. Although, near- and far-field optical approaches drastically improve image resolution, they still present numerous drawbacks, which include technical difficulties related to probe preparation (near-field) or potentially damaging light intensities (far-field).

The aforementioned shortcomings of high-resolution optical microscopy can be overcome to a great extent by photonic force microscopy (PFM). PFM employs a strongly focused near-infrared (NIR) laser light to hold a dielectric or metallic particle as a local probe. Such an optical trap enables confining a mesoscopic particle and track its three-dimensional (3D) thermal fluctuations in the surrounding environment, e.g., a viscous liquid. Therefore, besides offering 3D near-field imaging, PFM also reports on other important quantities concerning the local mechanical properties, including force and viscosity as well as dynamical properties of the surrounding medium. This additional information is derived from the careful

analysis of the so-called Brownian motion of the trapped single-particle probe that collides with thermally activated surrounding molecules.

At present, the most promising nonlinear, light-emitting nanoprobes that have been shown to be optically manipulable are nanowires made of perovskite alkaline niobates (e.g., KNbO₃)^{1,2} or indium phosphide.³ These nanowires are able to convert the continuous infrared (IR) light energy of the optical trap into one sharp visible line at half the excitation wavelength by a second-harmonic generation (SHG) process. Long KNbO₃ nanowires have potential application for near-field probing.¹ In particular, it was shown to be possible to excite organic fluorescent molecules, such as nucleic acid binding POPO-3 dyes, by a direct energy transfer from the trapped KNbO₃ nanowire emitting the SHG light.¹ However, SHG requires relatively high levels of IR power⁴ and challenges remain concerning preparation of SHG probes having controlled sizes and shapes suitable for optical manipulation.^{1,2}

Light-upconversion systems, which are capable of converting low-energy IR or NIR incident photons to higher energy emission, are increasingly gaining attention as novel probes for analytics in biological environments, quantitative microscopy, and bioimaging.⁵ In particular, lanthanide-doped upconversion luminescent nanoparticles (UCNPs) display the unique

Received: May 28, 2014

Published: November 5, 2014

property of emitting visible light following photoexcitation with NIR laser light.⁶ Such an upconversion photoluminescence (UCL) mechanism is generally not available for existing endogenous and exogenous fluorophores, offering UCNPs various distinctive characteristics for optical biomedical imaging, such as minimal autofluorescence background, large anti-Stokes shifts (up to 500 nm), narrow emission bandwidths, high resistance to photobleaching, nonblinking, less light scattering, and deeper tissue penetration.^{7,8} Additional advantages over other light-emitting probes are their higher quantum yield and a tunable emission wavelength.

UCNPs and their microsized upconversion counterparts (UCPs) are now becoming commercially available in a wide range of shapes and sizes.^{9,10} Typically, characterization of their photophysical properties is done in bulk,^{9–12} and only a few studies of the properties of single upconversion particles have been reported.^{13–16}

Recently, the feasibility of 3D optical trapping of small-sized UCNPs (~ 26 nm in diameter) was demonstrated by Haro-González et al.¹⁷ In the present work, we developed a methodology based on PFM and high-frequency optical trapping interferometry^{18,19} to simultaneously study photophysical and morphological properties of single UCPs. We implemented two types of commercially available highly luminescent UCPs based on β -NaYF₄, which were nominally doped with Yb and Er. These two types of UCPs were synthesized by two different technological pathways, i.e., the flame-fusion method and hydrothermal standard Schlenk technique, which resulted in two markedly different particle morphologies, that is, random and well-defined (hexagonal plate) shapes, respectively.

The rationale behind investigating UCPs having different morphologies, yet revealing similar photo-optical properties under experimental conditions of PFM, was imposed by the adopted procedure of calibration of the Brownian motion for particles of arbitrary shapes. In particular, first, we developed the calibration procedure for a particle having well-defined morphology (hexagonal plate), and then, the protocol was extended to UCPs of random shapes.

Our PFM experimental setup enabled us to investigate the UCL properties of UCPs at the single-particle level, at very high NIR laser power densities, up to 14.7 MW cm^{-2} , and revealed strong peaks of visible light emission related to the upconversion transitions within the electronic manifold of Er³⁺. We also observed additional, well-distinguished, although definitely much weaker UCL peaks, which were enhanced by the high laser power density. Moreover, unlike in bulk studies of UCPs, in PFM, interactions with neighboring particles could be avoided, thus minimizing distortions in UCL spectra of individual UCPs. Finally, the exact analysis of Brownian fluctuations of trapped single UCPs made it possible to evaluate the best-suited morphology of such particles for applications as near-field luminescent Brownian probes.

RESULTS AND DISCUSSION

To investigate the Brownian fluctuations of an optically trapped particle with $1 \mu\text{s}$ temporal and 1 nm spatial resolutions, we used a custom-built PFM setup.²⁰ It consists of an ultrastable inverted light microscope with a 3D sample positioning stage, a 1064 nm laser (IRCL-500-1064-S, Crystalaser, USA) for optical trapping, and a quadrant photodiode (QPD), model G6849 from Hamamatsu Photonics, Japan, for high-resolution as well as time-resolved position detection.

The PFM setup was modified to detect and measure nonlinear optical effects emitted by a single optically trapped particle excited directly by the 1064 nm trapping beam in continuous wave (CW) mode. In order to perform high-sensitivity photoluminescence detection, a spectrofluorometer (USB2000-FL-450, Ocean Optics Inc., USA) and an electron multiplying charge-coupled device (EMCCD, iXon^{EM}+897, Andor Technology, United Kingdom) camera were added (Figure 1).

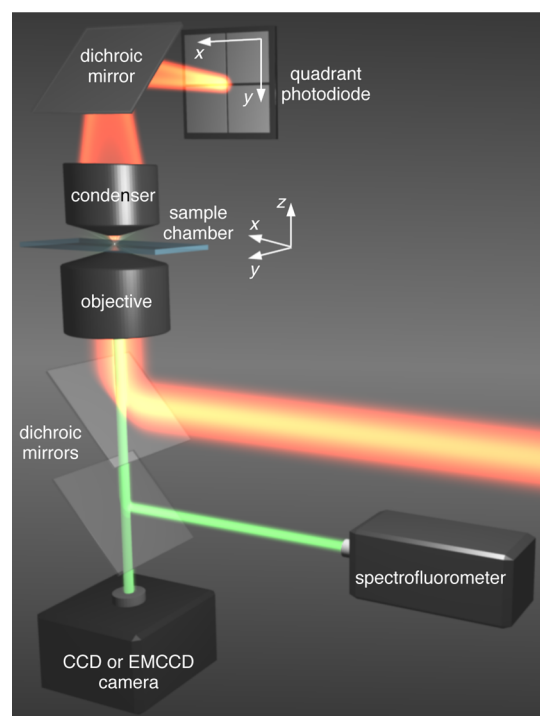


Figure 1. Schematic layout of the laser light pathways for particle trapping (orange light path) and for UCL detection (green light path). The Brownian motion of the trapped UCP was monitored with a QPD. The UCL spectra were acquired with a fiber-coupled spectrofluorometer. The trapped particle can be visualized with a CCD or an EMCCD camera. The NIR laser power can be varied by selected neutral density filters (see Supporting Information for more details).

Two types of lanthanide-doped samples with similar Yb/Er ratios were studied: (i) polycrystalline NaYF₄:22%Yb,2%Er UCPs having random shapes, edges, and sizes ranging from hundreds of nanometers to a few micrometers⁹ (Figure 2a) and (ii) the highly monodisperse, monocrystalline NaYF₄:20%Yb,2%Er plates of hexagonal shape, with edge lengths of ~ 230 nm and a thickness of ~ 120 nm¹⁰ (Figure 2b). UCPs of the first type, PTIR550/F, were bought from Phosphor Technology Ltd., Stevenage, England. These UCPs comprise polycrystalline NaYF₄:22%Yb,2%Er UCPs ground from bulk-grown crystals obtained by the flame-fusion method. UCPs of the second type were purchased from Intelligent Solutions Inc., Princeton, NJ, USA. These UCPs comprise monocrystalline NaYF₄:20%Yb,2%Er plates of hexagonal shape synthesized by standard Schlenk techniques.¹⁰ The as-received random shape UCPs were tip-sonicated to achieve stable suspensions in water, whereas the monodispersed hexagonal shape UCPs were dispersed in water using a sonication bath (see Supporting Information for more details).

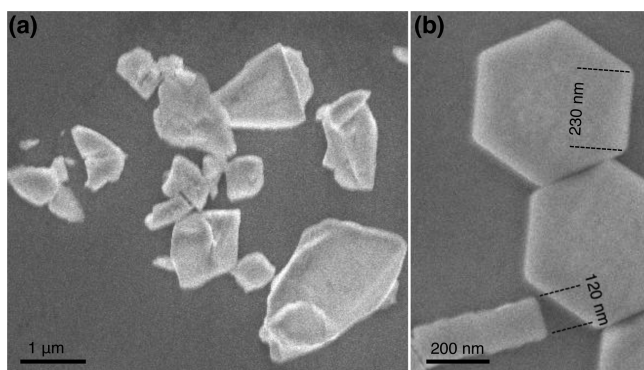


Figure 2. High-resolution scanning electron microscopy images of (a) random and (b) hexagonal shape UCPs. The detector for secondary electrons was placed 3 mm from the surface sample, and the energy of the excitation electrons was 3 keV for high-resolution imaging of the particles.

To study the UCL properties at the single-particle level, a dispersed aqueous solution of UCPs was first introduced into the sample chamber of our PFM. Next, the UCPs were allowed to sediment to the bottom surface. A single UCP was then selected by optical microscopy and picked up with the optical trap away from the bottom surface of the sample chamber. To make sure that we trapped a single UCP, during the experiment, we continuously checked the UCL spectra and monitored the Brownian motion. In particular, the amplitude of the UCL spectrum becomes higher when a second UCP particle enters the optical trap (see Supporting Information for more details). Finally, the UCL intensity spectrum of each optically trapped UCP excited by the NIR trapping laser was recorded. Figure 3a shows typical UCL intensity spectra for a random and hexagonal shape UCP trapped at different laser power densities Φ_{laser} . The laser power density was calculated knowing the $1/e^2$ radius $w_0 = 451 \text{ nm}^{21}$ and the laser power, P_{laser} , as $P_{\text{laser}}/(\pi w_0^2)$. The measurements were performed at room temperature. According to the model developed by E. J. G. Peterman et al. for polystyrene and silica microspheres,²² one can expect the temperature increase in the fluid adjacent to the particle to be $\sim 2 \text{ }^\circ\text{C}$ for the maximum laser power (94 mW) we used (see Supporting Information for more details). The UCL emission spectrum of a single optically trapped UCP exhibits a multicolored spectrum with nine distinguishable emission bands centered around 408.6, 469, 503.6, 525.4, 549.2, 616.1, 657, 697.8, and 841.9 nm. The wavelength for each emission band does not change because it is dopant- but not shape-dependent. Interestingly, the green light emitted by the trapped hexagonal plate is less quenched than for random shape particles (Figure 3a, black line).

The UCL intensity spectrum (Figure 3a) originates from the upconversion process between Yb^{3+} as a donor and Er^{3+} as an acceptor.²³ Peaks located at 408.6, 525.4, 549.2, and 657 nm are respectively attributed to the radiative transitions from the $^2\text{H}_{9/2}$, $^2\text{H}_{11/2}$, $^4\text{S}_{3/2}$, and $^4\text{F}_{9/2}$ excited states to the $^4\text{I}_{15/2}$ ground state of Er^{3+} (Figure 3b). These transitions were also visible in bulk measurements performed at low laser power densities.⁹ In contrast, the blue emission peaks around 469 and 503.6 nm matching the intrastate transitions $^2\text{K}_{15/2} \rightarrow ^4\text{I}_{13/2}$ and $^4\text{G}_{11/2} \rightarrow ^4\text{I}_{13/2}$ and the red peaks at 616.1 and 697.8 nm corresponding to the intrastate transitions $^4\text{G}_{11/2} \rightarrow ^4\text{I}_{11/2}$ and $^2\text{H}_{9/2} \rightarrow ^4\text{I}_{11/2}$, respectively, have not been observed in bulk measurements performed using much lower laser power densities.^{9,10}

Previously, the emission peaks at 697.8 and 841.9 nm have also been reported for similar particles measured at moderate power densities up to $\sim 300 \text{ W cm}^{-2}$.²⁴ In addition, investigations at the single-particle level have revealed the peak at 697.8 nm for a laser power density of $\sim 625 \text{ kW cm}^{-2}$.¹³ Thus, our measurements indicate that the three intrastate transitions at 469, 503.6, and 616.1 nm are exclusively visible due to a marked enhancement of their respective amplitudes by high laser power densities (up to 14.7 MW cm^{-2}) of our PFM setup. Interestingly, as can be seen in Figure 3b, the intensity of the NIR peak located at 841.9 nm, which matches three different intrastate transitions corresponding to $^4\text{G}_{9/2} \rightarrow ^4\text{F}_{9/2}$, $^2\text{H}_{9/2} \rightarrow ^4\text{I}_{9/2}$, and $^4\text{S}_{3/2} \rightarrow ^4\text{I}_{13/2}$, is also enhanced.

Even though we associated the UCL peaks at 469 and 503.6 nm with intrastate transitions of the 4f electron manifold of the Er^{3+} ions, they might also originate from impurities. However, available data on the purity of the studied UCPs do not suggest the presence of trace amounts of other lanthanides, which might contribute to these UCL peaks.^{9,10,25}

UCPs were exposed to variable laser power densities to evaluate their UCL emission. To this end, one representative and relatively large UCP of random shape ($\sim 1.2 \text{ }\mu\text{m}$) was trapped by the laser beam of the PFM, and its photoluminescence was measured as a function of laser power density, Φ_{laser} . Figure 3c shows the emitted UCL power, P_{UCL} , of the five major peaks (469, 525.4, 549.2, 657, and 697.8 nm) as a function of Φ_{laser} (see Supporting Information for the calculation of P_{UCL}). We chose a rather large UCP to assess over a broad laser power range the otherwise too weak light blue and dark red emission bands, centered around 469 and 697.8 nm, respectively. The strong laser power densities reached in the tightly focused laser beam of the optical trap allowed studying the highest energy electronic state excitable through the upconversion process (Figure 3b). As can be seen in Figure 3a and c, the UCL intensity increases with Φ_{laser} . Similar behavior of increasing UCL at very high laser power densities was observed by Gargas et al.¹⁶ The lowest power density ($\Phi_{\text{laser}} = 0.0867 \text{ MW cm}^{-2}$) corresponds to the minimal laser power necessary for trapping, which essentially depends on the size of the particle. It is worth noting that the laser power densities employed in this experiment were much higher than those reported in similar studies so far.

In principle, UCL is excited by the sequential absorption of N photons according to the relation $P_{\text{UCL}} \propto \Phi_{\text{laser}}^N$. The values of N were derived from fits of the log–log plots of $P_{\text{UCL}}(\Phi_{\text{laser}})$ (Figure 3c, black lines).^{24,26} At very low Φ_{laser} , far below trapping conditions, $2 < N < 3$ is typically observed in bulk, indicating a mixed two- or three-photon process.^{24,26} At the high excitation densities necessary for trapping ($0.07 \text{ MW cm}^{-2} \lesssim \Phi_{\text{laser}} \lesssim 1 \text{ MW cm}^{-2}$), we observe that N is reduced to ~ 1 due to saturation of the UCL process, except for the light blue emission band, which still exhibits a three-photon upconversion process, with $N \approx 3$ (Figure 3c). Further increasing the trapping strength yields $N < 1$, thus pointing to UCL quenching due to a lack of phonons.^{26,27} Nevertheless, even under such extreme conditions after 2 min of illumination at the highest power density, $\Phi_{\text{laser}} = 14.7 \text{ MW cm}^{-2}$, the UCP remained stable and only very low bleaching with no blinking was observed (see Supporting Information). This is in contrast to quantum dots (QDs)²⁸ and organic dyes.²⁹

Further manipulation and characterization of a single UCP were achieved in the optical trap, which was linearly polarized in the xy -plane perpendicular to the beam axis z . As the laser

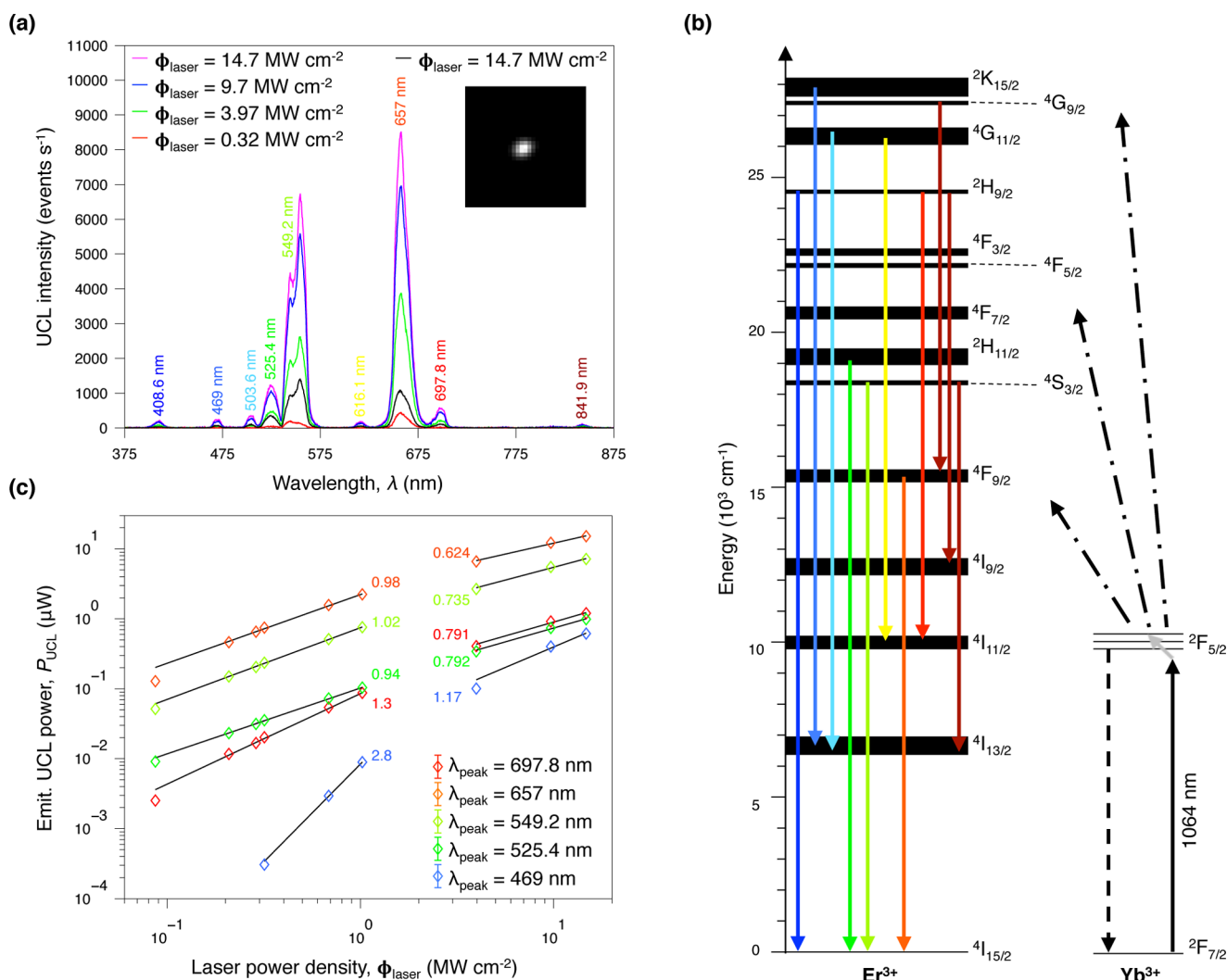


Figure 3. (a) Evolution of the UCL spectra from a single UCP as a function of the laser power density, Φ_{laser} , trapped at 0.32 (red trace), 3.97 (green trace), 9.7 (blue trace), and 14.7 (magenta trace) MW cm^{-2} , for a random shape UCP, and at 14.7 (black trace) MW cm^{-2} for a hexagonal shape UCP. All spectra were recorded using integration time $\mathcal{T}_{\text{int}} = 0.5$ s, and the particles were trapped in water. Inset: Photoluminescent EMCCD image of a single trapped hexagonal UCP. (b) Representation of the *f*-shell electronic levels of Yb^{3+} and Er^{3+} atoms, showing the energy transfer UC processes (indicated by three dash-dotted black arrows) responsible for photoluminescence after NIR excitation (indicated by a continuous black arrow) of the ${}^2\text{F}_{5/2}$ level of Yb^{3+} . A phonon (indicated by a continuous gray arrow) is needed to excite the ${}^2\text{F}_{5/2}$ level of Yb^{3+} . The black dotted line represents the radiative relaxation of Yb^{3+} . The nine colored arrows correspond to the peaks in the UCL spectrum shown in (a). (c) Log–log representation of the UCL emitted power from the representative random shape particle for its five major peaks. The corresponding exponents of the power law (N) for each emitted wavelength are shown adjacent to the plots. All spectra were recorded with integration times ranging from 0.05 to 5 s.

light carries linear and angular momentum that is transferred to the particle, the optical trap exerts not only a restoring force but also a restoring torque on the geometrically anisotropic particle.^{30,31} All particles studied here align spontaneously with the laser polarization in the *xy*-plane of the trap and exhibit only small-angle oscillations around their equilibrium orientation. The remaining Brownian fluctuations of the trapped UCP are detected by the QPD.

When a UCP is trapped, the large-angle rotational Brownian motion is strongly suppressed by the optical restoring torque and short-time fluctuations are dominated by the translational Brownian motion.³² Then, the hydrodynamic vortex, which develops by momentum exchange between the fluctuating particle and the surrounding fluid, influences also Brownian motion. For a spherical particle of radius R_s , the hydrodynamic vortex propagates around the particle in all three dimensions

with one characteristic time constant, $\tau_f = \rho_s R_s / \eta_f$ where ρ_f is the density and η_f the viscosity of the fluid.¹⁹ In contrast, for a nonspherical UCP, the *x*- and *y*-components of translational Brownian motion are anisotropic and yield two characteristic time constants, $\tau_{f,i} = \rho_f R_{e,i}^2 / \eta_f$ with $i = x, y$. $R_{e,x}$ and $R_{e,y}$ correspond to the effective radii along directions *x* and *y*, respectively, which are defined by the axis of the QPD (Figure 1).

As shown in Figure 4a, the time constants $\tau_{f,x}$ and $\tau_{f,y}$ appear in the short-time power laws $(t/\tau_{f,i})^{-3/2}$ of the velocity autocorrelation function (VAF) along the *x*- and *y*-directions, respectively. The values of $\tau_{f,x}$ and $\tau_{f,y}$ are derived from the Brownian motion of the trapped UCP. At longer times, each VAF_{*i*} exhibits a zero-crossing, which is then followed by a quasi-exponential relaxation with a characteristic time $\tau_{K_i} = 6\pi\eta R_{e,i} / K_i$, due to the restoring forces of the optical trap, with stiffness

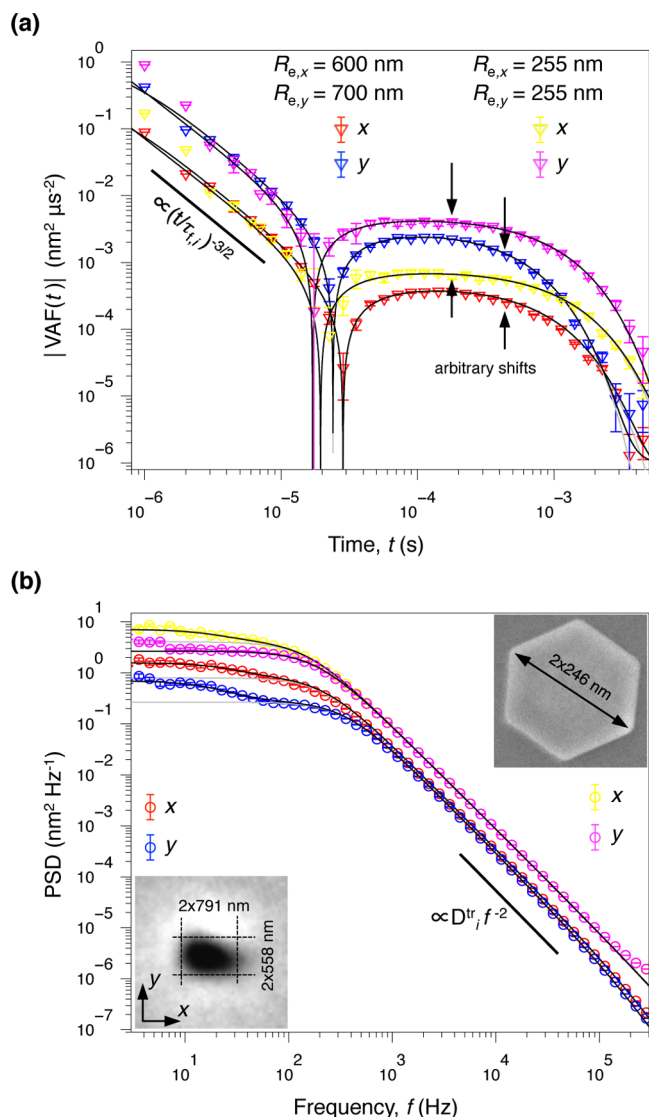


Figure 4. (a) Log–log plot of $|VAF|$ calibrated along the x - and y -directions for a random (red and blue data points) and hexagonal (yellow and magenta data points) shape UCP. (b) Log–log representation for the x - and y -components of the corresponding calibrated PSD. Insets: Images of the corresponding trapped UCPs. The gray lines indicate fitting based on the full hydrodynamic theory for a sphere,¹⁹ whereas the black lines take into account eqs 1 and 2 for the rotational motion. Both particles were trapped in water, at $\Phi_{\text{laser}} = 1.02 \text{ MW cm}^{-2}$ ($\rho_p = 4.21 \text{ kg m}^{-3}$, $\rho_f = 997.6 \text{ kg m}^{-3}$, and $\eta_f = 0.955 \text{ mPa s}$ at $T = 295 \text{ K}$). All data were blocked in 10 bins per decade, and error bars indicate the standard error of the mean values obtained from blocking.

K_r . Although the short-time fluctuations of the trapped UCP are primarily due to translational Brownian motion, the small-angle oscillations around its equilibrium orientation influence the long-time dynamics of the particle, as shown in the power spectral density (PSD) in Figure 4b for frequencies $f \lesssim 40 \text{ Hz}$. In principle, the influence of inertia of the fluid and the particle at these long times can be neglected for the rotational Brownian motion of an asymmetric particle.^{33,34} The rotational component of the VAF can be then expressed by a negative decaying exponential

$$VAF^{\text{rot}}(t) = -\frac{2D^{\text{rot}}}{\tau_{K_\phi}} e^{-t/\tau_{K_\phi}} \quad (1)$$

and the PSD results in a Lorentzian function

$$PSD^{\text{rot}}(f) = \frac{D^{\text{rot}}}{\pi f^2 \left(1 + \left(\frac{f_{K_\phi}}{f} \right)^2 \right)} \quad (2)$$

with the rotational diffusion constant, D^{rot} , and the time constant related to the optical torque, τ_{K_ϕ} . Expressions 1 and 2 are solutions of the overdamped Langevin equation, which is a first-order equation with no dependence on the particle mass.^{33,34}

Under our experimental conditions, coupling between translational and rotational motions is low, and both contributions occur at well-separated time scales. As a consequence, our data can be described by a superposition of the translational contribution, given by Franosch et al.,¹⁹ and the rotational contributions expressed by eqs 1 and 2 (Figure 4, black lines).

At short times, only translational motion needs to be considered. Thus, adapting the method developed for a sphere¹⁹ to asymmetric particles is sufficient to fit data to theory along the x - and y -directions (Figure 4, gray lines). The method consists in simultaneously fitting the long-time tail in the high-frequency window of the PSD, which is defined by the translational diffusion constant D_i^{tr} (Figure 4b). This yields effective radii $R_{e,x} = R_{e,y} = 255 \text{ nm}$ for a hexagonal plate, and $R_{e,x} = 600 \text{ nm}$ and $R_{e,y} = 700 \text{ nm}$ for a typical random shape UCP. Both results match the apparent sizes measured either from the CCD camera calibrated image (Figure 4b, bottom left inset) for the random shape particle or by high-resolution scanning electron microscopy for the hexagonal plate (Figure 4b, top right inset). As expected, the apparent radius along the x -axis of the random shape particle, $R_{a,x} = 791 \text{ nm}$, is close to the effective radius obtained by fitting the y -component of the Brownian motion $R_{e,y} = 700 \text{ nm}$, and concomitantly $R_{a,y} \approx R_{e,x}$. Translational diffusion of the random shape particle along the x -axis is larger because $R_{a,y}$ is smaller (Figure 4b, $D_x^{\text{tr}} > D_y^{\text{tr}}$, red and blue data points).

Apparent sizes, $2R_{a,x}$ and $2R_{a,y}$, are defined as measurable sizes along the respective x - and y -axis from the CCD camera calibrated image for a given orientation of the UCP in the optical trap. In contrast, the orientation of a hexagonal shape plate remained unknown because it was too small to be clearly visualized with the CCD camera. Nevertheless, at high frequencies we found the translational diffusion constants $D_x^{\text{tr}} = D_y^{\text{tr}}$, whereas at low frequencies, $f \lesssim 40 \text{ Hz}$, data could not be fitted by the theory for a spherical particle (Figure 4b, magenta and yellow data points).

Through the detection of Brownian motion of a single UCP held in the optical trap, a connection between the size of the particle and the intensity of its photoluminescence can be made. In Figure 5, we observe an increase of the emitted UCL power, P_{UCL} , of major emission bands at 525.4, 549.2, 657, and 697.8 nm (depicted in Figure 3a and b) with increasing UCP sizes. For an average effective radius $\langle R_e \rangle = (R_{e,x} + R_{e,y})/2$, below $\sim 400 \text{ nm}$, the light blue emission band at 469 nm is within the background noise of detection at the low laser power density $\Phi_{\text{laser}} = 1.02 \text{ MW cm}^{-2}$. This laser power density was

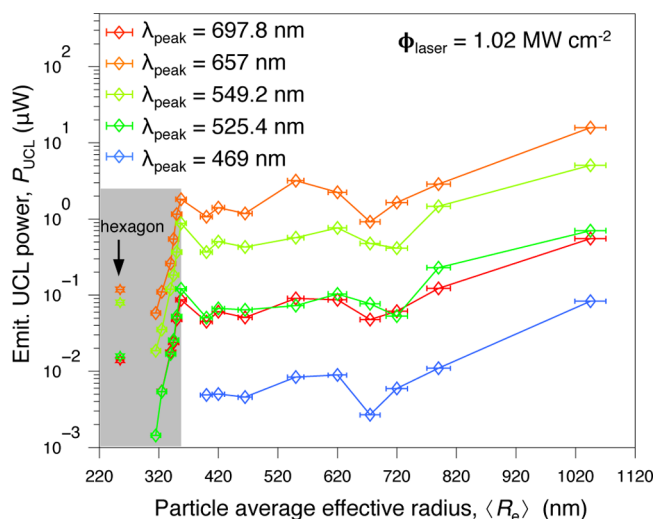


Figure 5. UCL power emitted by a trapped UCP as a function of its average effective radius $\langle R_e \rangle$. Only the five major peaks are represented (Figure 3c). The gray-shaded area highlights the region where P_{UCL} strongly depends on $\langle R_e \rangle$. Error bars originate from the uncertainty in reading out τ_{eff} .

employed to probe $\langle R_e \rangle$ for all particles investigated in Figure 5. The very steep increase of P_{UCL} below $\langle R_e \rangle = 357.5$ nm (Figure 5a, gray-shaded area) can be explained by the ratio of the particle and laser beam sizes at the trapping position. As long as $\langle R_e \rangle < w_0$, with $w_0 = 451$ nm being the $1/e^2$ radius of the focused trapping laser,²¹ any radial variation in the excitation density has drastic effects on P_{UCL} .²⁶ Furthermore, defect-induced quenching becomes more important for smaller ratios, $\langle R_e \rangle/w_0$. Such quenching is clearly higher for a random shape and polycrystalline UCP than for a monocrystalline and hexagonal shape UCP with well-defined edges, which exhibits therefore a more efficient upconversion process, despite its smaller size^{10,35,36} (Figure 5). As soon as $\langle R_e \rangle \gtrsim w_0$, the UCP sizes begin to exceed the laser beam diameter and then the thermal fluctuations influence less P_{UCL} (Figure 5, plateau at $\langle R_e \rangle > 357.5$ nm).

The results presented in Figure 5 can also allow tailoring the best-suited UCP morphologies for performing energy transfer in fluorescence microscopy from a single UCP to an adjacent chromophore with subwavelength resolution. In particular, the appropriate size of UCP has to be comparable to the size of the emission volume in a two-photon excitation (TPE) process, directly induced by the focused laser beam. In the case of our PFM operating at 1064 nm this emission volume is defined by the full width at half-maximum ($\text{fwhm}_0 = 345$ nm and $\text{fwhm}_z = 866$ nm).³⁷ Matching the UCP size and the TPE volume enables the energy transfer to dominate oversimple TPE processes. To further improve the spatial resolution, tuning the UCL emission by designing core/shell-structured upconversion particles is worth investigating.^{38,36}

CONCLUSIONS

In summary, we characterized in detail, at the single-particle level, the upconversion properties of random and hexagonal shape particles of $\text{NaYF}_4:\text{Yb},\text{Er}$. These nano/microsized UCPs could be easily manipulated and revealed efficient nonlinear multicolor UCL, while being trapped by the NIR laser beam of the PFM. Our results indicate also that the amplitudes of individual visible UCL emission bands depend on the laser

power density as well as the size and shape of the particles. In particular, the hexagonal plates exhibit a much stronger UCL emission than random shape particles of comparable sizes. This might be due to a lower content of structural defects in the highly crystalline structures. Moreover, under high laser power densities UCPs were photostable and revealed no blinking. In addition, the analysis of the Brownian motion of the trapped UCP allowed us to precisely measure its two-dimensional sizes. This was done by exploiting the short time dynamics of thermal fluctuations of the UCP through the simultaneous fitting of the VAF and PSD.

In brief, further research in this domain will broaden the application field of $\text{NaYF}_4:\text{Yb},\text{Er}$ nanoparticles from photoluminescent single-particle probes to such applications as nanolight sources for multiplexed molecule sensing at the nanoscale with subwavelength resolution. In biomedically oriented studies, the novel microscopic methodology proposed herein can provide a deeper insight into mechanical and microrheological properties of intracellular components and interactions. In particular, due to the implementation of PFM, stiffness, viscosity, and exerted forces can be evaluated with nanometer spatial and microsecond temporal resolutions.

ASSOCIATED CONTENT

Supporting Information

Further details on the PFM instrument (Figure S1), morphologies of the UCPs, optical trapping of single UCPs, laser-induced heating in PFM, calibration of the spectrofluorometer (Figures S2 and S3), quantification of the UCL spectrum (Figure S4), and UCL bleaching (Figure S5) can be found in the Supporting Information. This material is available free of charge via the Internet at <http://pubs.acs.org>.

AUTHOR INFORMATION

Corresponding Author

*E-mail: flavio.mor@epfl.ch. Phone: +41 (21) 693 4438. Fax: +41 (21) 693 4470.

Notes

The authors declare no competing financial interest.

ACKNOWLEDGMENTS

We thank S. Haacke and H. U. Güdel for useful discussions. S.J. and F.M.M. acknowledge support from the National Centre of Competence in Research (NCCR Nano-Bio, Project 1.4) and the Swiss National Science Foundation (SNSF, project numbers 206021_121396 and 200021_143703). F.M.M. was supported by the National Competence Center in Biomedical Imaging (NCCBI). The research was also cofinanced by the SNSF through the Nano-Tera.ch focused NTF project "NanoUp".

REFERENCES

- (1) Nakayama, Y.; Pauzauskis, P. J.; Radenovic, A.; Onorato, R. M.; Saykally, R.; Liphardt, J.; Yang, P. Tunable nanowire nonlinear optical probe. *Nature* **2007**, *447*, 1098–1102.
- (2) Dutto, F.; Raillon, C.; Schenk, K.; Radenovic, A. Nonlinear optical response in single alkaline niobate nanowires. *Nano Lett.* **2011**, *11*, 2517–2521.
- (3) Reece, P. J.; Paiman, S.; Abdul-Nabi, O.; Gao, Q.; Gal, M.; Tan, H. H.; Jagadish, C. Combined optical trapping and microphotoluminescence of single InP nanowires. *Appl. Phys. Lett.* **2009**, *95*, 1–3.
- (4) Cohen, B. E. Beyond fluorescence. *Nature* **2010**, *467*, 407–408.

- (5) Gorris, H. H.; Wolfbeis, O. S. Photon-upconverting nanoparticles for optical encoding and multiplexing of cells, biomolecules, and microspheres. *Angew. Chem., Int. Ed.* **2013**, *52*, 3584–3600.
- (6) Esipova, T. V.; Ye, X.; Collins, J. E.; Sakadžić, S.; Mandeville, E. T.; Murray, C. B.; Vinogradov, S. A. Dendritic upconverting nanoparticles enable in vivo multiphoton microscopy with low-power continuous wave sources. *Proc. Natl. Acad. Sci. U.S.A.* **2012**, *109*, 20826–20831.
- (7) Pantazis, P.; Maloney, J.; Wu, D.; Fraser, S. E. Second harmonic generating (SHG) nanoprobe for in vivo imaging. *Proc. Natl. Acad. Sci. U.S.A.* **2010**, *107*, 14535–14540.
- (8) Mader, H. S.; Kele, P.; Saleh, S. M.; Wolfbeis, O. S. Upconverting luminescent nanoparticles for use in bioconjugation and bioimaging. *Curr. Opin. Chem. Biol.* **2010**, *14*, 582–596.
- (9) Soukka, T.; Kuningas, K.; Rantanen, T.; Haasslahti, V.; Lövgren, T. Photochemical characterization of up-converting inorganic lanthanide phosphors as potential labels. *J. Fluoresc.* **2005**, *15*, 513–528.
- (10) Ye, X.; Collins, J. E.; Kang, Y.; Chen, J.; Chen, D. T. N.; Yodh, A. G.; Murray, C. B. Morphologically controlled synthesis of colloidal upconversion nanophosphors and their shape-directed self-assembly. *Proc. Natl. Acad. Sci. U.S.A.* **2010**, *107*, 22430–22435.
- (11) Wang, F.; Liu, X. Recent advances in the chemistry of lanthanide-doped upconversion nanocrystals. *Chem. Soc. Rev.* **2009**, *38*, 976–989.
- (12) Wang, F.; Banerjee, D.; Liu, Y.; Chen, X.; Liu, X. Upconversion nanoparticles in biological labeling, imaging, and therapy. *Analyst* **2010**, *135*, 1839–1854.
- (13) Schietinger, S.; de S. Menezes, L.; Lauritzen, B.; Benson, O. Observation of size dependence in multicolor upconversion in single Yb^{3+} , Er^{3+} codoped NaYF_4 nanocrystals. *Nano Lett.* **2009**, *9*, 2477–2481.
- (14) Wu, S.; Han, G.; Milliron, D. J.; Aloni, S.; Altoe, V.; Talapin, D. V.; Cohen, B. E.; Schuck, P. J. Non-blinking and photostable upconverted luminescence from single lanthanide-doped nanocrystals. *Proc. Natl. Acad. Sci. U.S.A.* **2009**, *106*, 10917–10921.
- (15) Schietinger, S.; Aichele, T.; Wang, H.-Q.; Nann, T.; Benson, O. Plasmon-enhanced upconversion in single $\text{NaYF}_4:\text{Yb}^{3+}/\text{Er}^{3+}$ codoped nanocrystals. *Nano Lett.* **2010**, *10*, 134–138.
- (16) Gargas, D. J.; Chan, E. M.; Ostrowski, A. D.; Aloni, S.; Altoe, M. V. P.; Barnard, E. S.; Sanii, B.; Urban, J. J.; Miliron, D. J.; Cohen, B. E.; Schuck, P. J. Engineering bright sub-10-nm upconverting nanocrystals for single-molecule imaging. *Nat. Nanotechnol.* **2014**, *9*, 300–305.
- (17) Haro-González, P.; del Rosal, B.; Maestro, L. M.; Rodríguez, E. M.; Naccache, R.; Capobianco, J. A.; Dholakia, K.; Solé, J. G.; Jaque, D. Optical trapping of $\text{NaYF}_4:\text{Er}^{3+}, \text{Yb}^{3+}$ upconverting fluorescent nanoparticles. *Nanoscale* **2013**, *5*, 12192–12199.
- (18) Gittes, F.; Schmidt, C. F. Interference model for back-focal-plane displacement detection in optical tweezers. *Opt. Lett.* **1998**, *23*, 7–9.
- (19) Franosch, T.; Grimm, M.; Belushkin, M.; Mor, F. M.; Foffi, G.; Forró, L.; Jeney, S. Resonances arising from hydrodynamic memory in Brownian motion. *Nature* **2011**, *478*, 85–88.
- (20) Jeney, S.; Mor, F.; Köszali, R.; Forró, L.; Moy, V. T. Monitoring ligand-receptor interactions by photonic force microscopy. *Nanotechnology* **2010**, *21*, 1–8.
- (21) Smith, S. P.; Bhalotra, S. R.; Brody, A. L.; Brown, B. L.; Boyda, E. K.; Prentiss, M. Inexpensive optical tweezers for undergraduate laboratories. *Am. J. Phys.* **1999**, *67*, 26–35.
- (22) Peterman, E. J. G.; Gittes, F.; Schmidt, C. F. Laser-induced heating in optical traps. *Biophys. J.* **2003**, *84*, 1308–1316.
- (23) Renero-Lacuna, C.; Martín-Rodríguez, R.; Valiente, R.; González, J.; Rodríguez, F.; Krämer, K. W.; Güdel, H. U. Origin of the high upconversion green luminescence efficiency in $\beta\text{-NaYF}_4:2\%\text{Er}^{3+}, 20\%\text{Yb}^{3+}$. *Chem. Mater.* **2011**, *23*, 3442–3448.
- (24) Suyver, J. F.; Aebischer, A.; Garca-Revilla, S.; Gerner, P.; Güdel, H. U. Anomalous power dependence of sensitized upconversion luminescence. *Phys. Rev. B* **2005**, *71*, 125123–125131.
- (25) Wang, F.; Han, Y.; Lim, C.; Lu, Y.; Wang, J.; Xu, J.; Chen, H.; Zhang, C.; Hong, M.; Liu, X. Simultaneous phase and size control of upconversion nanocrystals through lanthanide doping. *Nature* **2010**, *463*, 1061–1065.
- (26) Pollnau, M.; Gamelin, D. R.; Lüthi, S. R.; Güdel, H. U.; Hehlen, M. P. Power dependence of upconversion luminescence in lanthanide and transition-metal-ion systems. *Phys. Rev. E* **2000**, *61*, 3337–3346.
- (27) Shan, J.; Uddi, M.; Wei, R.; Yao, N.; Ju, Y. The hidden effects of particle shape and criteria for evaluating the upconversion luminescence of the lanthanide doped nanophosphors. *J. Phys. Chem. C* **2010**, *114*, 2452–2461.
- (28) Jauffred, L.; Oddershede, L. B. Two-photon quantum dot excitation during optical trapping. *Nano Lett.* **2010**, *10*, 1927–1930.
- (29) Patterson, G. H.; Piston, D. W. Photobleaching in two-photon excitation microscopy. *Biophys. J.* **2000**, *78*, 2159–2162.
- (30) Friese, M. E. J.; Nieminen, T. A.; Heckenberg, N. R.; Rubinsztein-Dunlop, H. Optical alignment and spinning of laser-trapped microscopic particles. *Nature* **1998**, *394*, 348–350.
- (31) Higurashi, E.; Ukita, H.; Tanaka, H.; Ohguchi, O. Optically induced rotation of anisotropic microobjects fabricated by surface micromachining. *Appl. Phys. Lett.* **1994**, *64*, 2209–2210.
- (32) Han, Y.; Alsayed, A. M.; Nobili, M.; Zhang, J.; Lubensky, T. C.; Yodh, A. G. Brownian motion of an ellipsoid. *Science* **2006**, *314*, 626–630.
- (33) Maragó, O. M.; Jones, P. H.; Bonaccorso, F.; Scardaci, V.; Guccardi, P. G.; Rozhin, A. G.; Ferrari, A. C. Femtonewton force sensing with optically trapped nanotubes. *Nano Lett.* **2008**, *8*, 3211–3216.
- (34) Maragó, O. M.; Bonaccorso, F.; Saija, R.; Privitera, G.; Guccardi, P. G.; Latì, M. A.; Calogero, G.; Jones, P. H.; Borghese, F.; Denti, P.; Nicolosi, V.; Ferrari, A. C. Brownian motion of graphene. *ACS Nano* **2010**, *4*, 7515–7523.
- (35) Bai, X.; Song, H.; Pan, G.; Lei, Y.; Wang, T.; Ren, X.; Lu, S.; Dong, B.; Fan, L. Size-dependent upconversion luminescence in $\text{Er}^{3+}/\text{Yb}^{3+}$ -codoped nanocrystalline yttria: saturation and thermal effects. *J. Phys. Chem. C* **2007**, *111*, 13611–13617.
- (36) Mai, H.-X.; Zhang, Y.-W.; Sun, L.-D.; Yan, C.-H. Highly efficient multicolor up-conversion emissions and their mechanisms of monodisperse $\text{NaYF}_4:\text{Yb}, \text{Er}$ core and core/shell-structured nanocrystals. *J. Phys. Chem. C* **2007**, *111*, 13721–13729.
- (37) Zipfel, W. R.; Williams, R. M.; Webb, W. W. Nonlinear magic: multiphoton microscopy in the biosciences. *Nat. Biotechnol.* **2003**, *21*, 1369–1377.
- (38) Yi, G.-S.; Chow, G.-M. Water-soluble $\text{NaYF}_4:\text{Yb}, \text{Er}(\text{Tm})/\text{NaYF}_4/\text{polymercore/shell/shell}$ nanoparticles with significant enhancement of upconversion fluorescence. *Chem. Mater.* **2007**, *19*, 341–343.